

OPEN ACCESS

Repository of the Max Delbrück Center for Molecular Medicine (MDC)
in the Helmholtz Association

<http://edoc.mdc-berlin.de/15564>

Blood flow drives lumen formation by inverse membrane blebbing during angiogenesis in vivo

Gebala, V. and Collins, R. and Geudens, I. and Phng, L.K. and Gerhardt, H.

This is the final version of the accepted manuscript. The original article has been published in final edited form in:

Nature Cell Biology
2016 APR; 18(4): 443-450
2016 FEB 29 (online publication date)
doi: [10.1038/ncb3320](https://doi.org/10.1038/ncb3320)

Publisher: [Macmillan Publishers](#) (Springer Nature)

Copyright © 2016 The Author(s)

Note: Supplementary figures and videos are available in the [online version of the paper](#)

1 Blood flow drives lumen formation by inverse membrane blebbing during
2 angiogenesis *in vivo*

3

4 Véronique Gebala^{1,2}, Russell Collins², Ilse Geudens³, Li-Kun Phng^{3,4*}, Holger
5 Gerhardt^{2,3,5,6*}

6

7 1, The Francis Crick Institute, Lincoln's Inn Fields Laboratory, 44 Lincoln's Inn
8 Fields, London WC2A 3LY, UK

9 2, Present address: Integrative Vascular Biology Laboratory, Max-Delbrück-Center
10 for Molecular Medicine in the Helmholtz Association (MDC), Robert-Rössle-Strasse
11 10, 13125 Berlin, Germany

12 3, Vascular Patterning Laboratory, Vesalius Research Center, VIB, Department of
13 Oncology, KU Leuven, Herestraat 49, 3000 Leuven, Belgium

14 4, Present address: Department of Cell Biology, National Cerebral and Cardiovascular
15 Center Research Institute, Osaka 565-8565, Japan

16 5, DZHK (German Center for Cardiovascular Research), partner site Berlin

17 6, Berlin Institute of Health (BIH), Berlin, Germany

18

19 *, These authors contributed equally to this work.

20

21 Correspondence should be addressed to H.G. (email: holger.gerhardt@mdc-berlin.de)

22

23 Abstract

24

25 How vascular tubes build, maintain and adapt continuously perfused lumens to meet
26 local metabolic needs remains poorly understood. Recent studies showed that blood
27 flow itself plays a critical role in the remodelling of vascular networks^{1,2}, and
28 suggested it is also required for lumenisation of new vascular connections^{3,4}.
29 However, it is still unknown how haemodynamic forces contribute to the formation of
30 new vascular lumens during blood vessel morphogenesis.

31 Here we report that blood flow drives lumen expansion during sprouting angiogenesis
32 *in vivo* by inducing spherical deformations of the apical membrane of endothelial
33 cells, in a process that we termed inverse blebbing. We show that endothelial cells
34 react to these membrane intrusions by local and transient recruitment and contraction
35 of actomyosin, and that this mechanism is required for single, unidirectional lumen
36 expansion in angiogenic sprouts.

37 Our work identifies inverse membrane blebbing as a cellular response to high external
38 pressure. We show that in the case of blood vessels such membrane dynamics can
39 drive local cell shape changes required for global tissue morphogenesis, shedding
40 light on a pressure-driven mechanism of lumen formation in vertebrates.

41

42 Blood vessels form a vast but highly structured network that pervades all organs in
43 vertebrates. During development as well as in pathological settings in adults, vascular
44 networks expand through a process known as sprouting angiogenesis. New blood
45 vessels form from the coordinated migration and proliferation of endothelial cells into
46 vascular sprouts. Subsequent fusion of neighbouring sprouts, defined as anastomosis,
47 then leads to the formation of new vascular loops, whose functionality relies on their
48 successful lumenisation and perfusion⁵. During anastomosis, endothelial lumens form
49 both through apical membrane invagination into single anastomosing cells
50 (unicellular lumen formation), and through *de novo* apical membrane formation at
51 their nascent junction (multicellular lumen formation)^{3,4}. Since the tip of endothelial
52 sprouts can be occupied by either one or several cells as they compete for the tip
53 position^{6,7}, we asked whether similar mechanisms of lumen formation apply to
54 unicellular and multicellular endothelial sprouts prior to anastomosis.

55 Using a zebrafish transgenic line expressing an mCherry-CAAX reporter for
56 endothelial plasma membrane (*Tg(kdr-l:ras-Cherry)*^{s916}), we imaged lumen formation
57 in tip cells as they sprout from the dorsal aorta (DA) to form the intersegmental
58 vessels (ISVs) from 30 hours post-fertilisation (hpf). We found that lumens expand in
59 sprouting ISVs prior to anastomosis, and do so by invagination of the apical
60 membrane either into single tip cells, or along cell junctions when the tip of a
61 sprouting ISV is shared between several cells (Fig. 1a,b).

62 To test if this mechanism of lumen formation is conserved in other vertebrates, we
63 performed immunolabelling of the apical membrane (ICAM-2, Intercellular Adhesion
64 Molecule 2) and cell junctions (ZO-1, Zona Occludens 1) in developing mouse retinas
65 at post-natal day 6 (P6). As in zebrafish ISVs, we observed that lumens are present
66 either as membrane invaginations into single tip cells, or between cells when they

67 share the tip position (Fig. 1c,d), suggesting that endothelial sprouts undergo both
68 unicellular and multicellular lumen formation in the mouse retina.

69 Whereas lumens form independently of blood flow during dorsal aorta formation⁸⁻¹⁰,
70 previous studies suggested both flow-independent and flow-dependent lumen
71 formation in ISVs¹¹ and during anastomosis^{3,4}. To test whether lumen expansion in
72 angiogenic sprouts requires blood perfusion, we treated *Tg(kdr-l:ras-Cherry)*^{s916}
73 embryos with a four-fold higher dose of tricaine methanesulfonate (4x tricaine) than
74 the dose normally used for anesthesia. Under these conditions, embryos show lower
75 heart rate, loss of blood flow and decreased blood pressure⁴. Upon the addition of 4x
76 tricaine mid-way through ISV lumenisation, lumens did not expand further and
77 eventually collapsed (Fig. 1e). However, when placed back in 1x tricaine at 2 days
78 post-fertilisation (dpf), the embryos recovered normal heartbeat, blood flow was re-
79 established (as assessed by the presence of circulating red blood cells) and lumens
80 expanded within the ISVs (Fig. 1e). Together, these data show that lumen expansion
81 in angiogenic sprouts is dependent on cardiac activity and thus on haemodynamics *in*
82 *vivo*.

83

84 Using mosaic expression of an endothelial-specific EGFP-CAAX reporter for plasma
85 membrane (*fli1ep:EGFP-CAAX*) and high spatial and temporal resolution imaging,
86 we discovered that apical membranes undergo rapid expansion through a process
87 reminiscent of membrane blebbing (Fig. 2a, panels B,C). Membrane blebs are plasma
88 membrane protrusions caused by local disruption of the actomyosin cortex or its
89 detachment from the plasma membrane¹²⁻¹⁶. Under cytoplasmic pressure, the
90 membrane in such actomyosin-free regions inflates from a neck into a spherical
91 protrusion. Depending on the context, blebs are either resolved by detachment (as

92 seen in apoptosis), forward movement of the cell (during cell migration), or through
93 recruitment and contraction of the actomyosin cortex on the inner side of the bleb
94 (bleb retraction, as seen in cell division)¹⁶. In endothelial cells, we observed blebbing
95 of the apical membrane during lumen expansion (Fig. 2a and Supplementary Video
96 1). These blebs however showed inverted polarity compared to previously described
97 blebs, with the apical membrane protruding into the cell body. Hence, we propose to
98 name this process “inverse membrane blebbing”. Following expansion, the inverse
99 blebs either retracted (Fig. 2a, panel B and black arrowheads in Fig. 2b) or persisted,
100 in particular as larger structures, leading to an expansion of the luminal compartment
101 (Fig. 2a, panel C and white arrowheads in Fig. 2b). Interestingly, persisting blebs
102 were only found at the tip of the growing lumen, therefore restricting lumen
103 expansion to this region of the cell. In contrast, the blebs arising on the lateral sides of
104 the lumen always retracted (Supplementary Video 1). Quantitative morphometric
105 analysis of inverse blebs showed that their size, expansion time and speed, as well as
106 retraction time and speed, are of the same order of magnitude than those of classical
107 blebs^{12,15} (Supplementary Fig. 1a-e). Similar membrane dynamics were observed
108 using a PLC δ -PH-RFP reporter for phosphatidylinositol-4,5-biphosphate (PIP₂), an
109 early apical determinant in epithelia¹⁷, confirming that inverse blebbing occurs
110 specifically at the apical membrane of endothelial cells (Supplementary Fig. 1f and
111 Supplementary Video 2).

112 Inverse blebs were observed at the apical membrane of both unicellular (Fig. 2a) and
113 multicellular (Fig. 2c and Supplementary Video 3) sprouts during lumen expansion.
114 However, because endothelial cell junctions are highly dynamic^{6,18,19} and accumulate
115 apical markers during lumenisation³ (Supplementary Video 2), we chose for clarity to

116 focus our subsequent analysis on unicellular lumens where non-junctional apical
117 membrane can clearly be distinguished.

118 In the mouse retina, stainings for ICAM-2 revealed the presence of two major lumen
119 configurations in angiogenic sprouts where the apical membrane appeared either
120 expanded (Fig. 2d, top panels, and Fig. 2e) or constricted (Fig. 2d, middle panels, and
121 Fig. 2e), suggesting that a similar mechanism of apical membrane blebbing might
122 take place during sprouting angiogenesis in mice.

123

124 In order to assess whether inverse blebbing is driven by blood pressure, blood flow
125 was stopped in single ISVs by laser ablating the connection of the sprouts to the
126 dorsal aorta (Fig. 3a). The loss of blood flow resulted in an immediate stop of apical
127 membrane blebbing and a gradual regression of the lumen (Fig. 3a and
128 Supplementary Video 4). Similar results were obtained by treating embryos with 4x
129 tricaine (Fig. 3b). Following 15-20 minutes of treatment, blood flow stopped (as
130 assessed by the absence of circulating red blood cells) and blebs could no longer be
131 observed at the apical membrane of lumenising cells (Fig. 3b, kymograph and panel
132 B, and Supplementary Video 5). When returned to 1x tricaine, embryos recovered
133 blood flow and re-expanded lumens by inverse blebbing (Fig. 3b, kymograph and
134 panel E, and Supplementary Video 5). Together, these experiments suggest that the
135 generation of inverse blebs depends on the positive pressure difference existing
136 between the luminal and the cytoplasmic sides of the apical membrane.

137 Importantly, unlike previous reports suggesting that lumens form in sprouting ISVs
138 through the fusion of intracellular vacuoles^{11,20,21}, we could not observe the formation
139 of any vacuolar structure in the cytoplasm of endothelial cells during phases of lumen
140 expansion (Fig. 2a and Supplementary Video 1). Isolated lumen fragments were only

141 seen arising from the local collapse of the lumen, and rapidly reconnected to the
142 growing lumen (Fig. 2a, panel D and Supplementary Video 1). The fact that such
143 collapse and regrowth events can be reproduced experimentally by stopping then
144 restarting blood flow (Fig. 3b and Supplementary Video 5) suggests that these events
145 occur during normal development following local variations in blood pressure. The
146 observation of a low number of large disconnected lumen fragments in angiogenic
147 sprouts in mouse retinas (Fig. 2d, bottom panels, and Fig. 2e) also suggests that the
148 apical membrane undergoes similar dynamics during mouse retina development.

149

150 In order to identify the molecular mechanism underlying bleb retraction, fluorescent
151 reporters for F-actin (Lifeact-EGFP and Lifeact-mCherry) and for the regulatory light
152 chain of non-muscle Myosin-II (Myl9b-EGFP) were expressed in wild-type or
153 *Tg(kdr-l:ras-Cherry)^{s916}* embryos. At 2 dpf, both reporters co-localised at the apical
154 membrane in perfused ISVs (Supplementary Fig. 2a, panel B), indicating that an
155 actomyosin cortex supports the apical membrane in small vessels. During lumen
156 formation, blebs expanded devoid of any F-actin or Myosin-II (Fig. 4a-d,
157 Supplementary Fig. 2b,c). In the event of retraction, F-actin polymerisation was
158 observed at the apical membrane all around the bleb surface, from the initiation of
159 retraction until its completion (Fig. 4a,b and Supplementary Video 6). Similarly,
160 Myosin-II was recruited to the cytoplasmic surface of the bleb during retraction (Fig.
161 4c,d and Supplementary Fig. 2b,c). Co-expression of F-actin and Myosin-II reporters
162 showed that Myosin-II is recruited to the apical membrane shortly after the initiation
163 of F-actin polymerisation (Fig. 4c,d). Together, these data suggest that the recruitment
164 and contraction of an actomyosin cortex at the apical membrane drives bleb retraction
165 during lumen expansion (Fig. 4j).

166 In order to test this hypothesis, we generated a non-phosphorylatable form of the
167 Myosin-II regulatory light chain (Myl9bAA) previously shown to act as a dominant-
168 negative²². In order to avoid any general and potentially deleterious effects during
169 earlier development, the expression of Myl9bAA-EGFP was restricted to single
170 endothelial cells and induced at the onset of lumen formation using the LexPR
171 expression system²³. Upon expression of Myl9bAA, we observed a significant
172 difference in the frequency of bleb retraction compared to control cells expressing the
173 wild-type form of Myl9b (Myl9b-EGFP), with a larger proportion of blebs showing
174 no or partial retraction (Fig. 4e). These data therefore confirm that actomyosin
175 contraction drives bleb retraction during lumen formation.

176 In order to test whether inverse membrane blebbing is, similarly to classical blebbing,
177 the result of the local detachment of the membrane from its underlying cortex²⁴, we
178 performed local laser ablation of the cortex at the apical membrane of lumenising
179 sprouts in *Tg(kdr-l:ras-Cherry^{s916};fli1ep:Lifect-EGFP)* embryos. By doing so, we
180 could induce the expansion of inverse blebs at the apical membrane of lumenising
181 vessels (Fig. 4f and Supplementary Video 7). This result suggests that local
182 detachment of the cortex from the apical membrane, in conjunction with blood
183 pressure, could be the trigger of inverse blebbing (Fig. 4j).

184 In mice, the imaging of retinas from Lifect-EGFP^{+/-wt} pups and of wild-type retinas
185 stained for non-muscle Myosin-IIA or phosphorylated Myosin Light Chain 2
186 (pMLC2) showed accumulation of actomyosin at the apical membrane in sprouting
187 cells (Fig. 4g-i), suggesting that a similar recruitment and contraction of actomyosin
188 could take place during lumen formation in angiogenic vessels in mice.

189

190 In order to assess whether apical membrane contractility is required for proper
191 lumenisation, we inhibited actomyosin contraction by expressing Myl9bAA from 30
192 hpf and checked ISVs for the presence of a lumen at 2 dpf. Quantification of ISVs
193 with Myl9bAA expression revealed a significant difference compared to control
194 embryos (Fig. 5a), with a decrease in the proportion of cells showing normal lumens.
195 Depending on their level of Myl9bAA expression, abnormal ISVs were either found
196 to be unlumenised or displayed dilated lumens (Fig. 5a,b). Live imaging from 30 hpf
197 showed that the absence of lumen was due to an inability of Myl9bAA-expressing
198 cells to expand lumens (Fig. 5c and Supplementary Video 8).

199 In order to gain a deeper mechanistic understanding of the effects of Myl9bAA
200 expression on the apical membrane dynamics, we performed fast imaging of both
201 unlumenised and dilated cells at 2 dpf (Fig. 5b and Supplementary Videos 9 and 10).
202 In both cases, the membrane dynamics was visibly affected by the expression of
203 Myl9bAA. In unlumenised ISVs, lumen initially expanded into Myl9bAA-expressing
204 cells but the apical membrane showed excessive and uncoordinated blebbing with
205 frequent disconnections of blebs from the membrane (Fig. 5b, arrowhead, and
206 Supplementary Video 9), therefore preventing lumen expansion. On the other hand,
207 dilated, partially lumenised cells were unable to fully retract blebs growing on the
208 lateral sides of the lumen (Fig. 4e,5b and Supplementary Video 10), leading to the
209 formation of side lumen branches (Fig. 5b, arrow, and Supplementary Video 10).
210 Together, these data show that sprouting cells require actomyosin contraction at the
211 apical membrane to control membrane deformations and ensure single, unidirectional
212 lumen expansion in response to blood pressure.

213

214 Our present results challenge the previous idea that sprouting cells expand lumens
215 independently of blood flow during angiogenesis *in vivo* through the generation and
216 fusion of intracellular vacuoles. Although endothelial cells are able to generate
217 lumens independently of blood flow *in vitro*²⁵ and during vasculogenesis⁸⁻¹⁰, we show
218 here that haemodynamic forces dynamically shape the apical membrane of single or
219 groups of endothelial cells during angiogenesis *in vivo* to form and expand new
220 lumenised vascular tubes. We find that this process relies on a tight balance between
221 the forces applied on the membrane and the local contractile responses from the
222 endothelial cells, as impairing this balance either way leads to lumen defects.

223 Our finding of inverse blebbing suggests that the process of blebbing, best studied in
224 cell migration and cytokinesis, does not require a specific polarity, but is likely
225 generally applicable to situations in which external versus internal pressure
226 differences challenge the stability and elasticity of the actin cortex. In the case of
227 endothelial cells, we describe a role for inverse blebbing in expanding the apical
228 membrane under pressure while ensuring unidirectional expansion of a single lumen
229 in angiogenic sprouts.

230 Our work more generally raises the question of the role of apical membrane
231 contractility in the adaptation to varying haemodynamic environments, both during
232 blood vessel morphogenesis, as connections form or remodel, and in pathological
233 settings. Our present work and previous studies^{26,27} highlight the importance of
234 balanced endothelial cell contractility in allowing the expansion and maintenance of
235 endothelial lumens during blood vessel development. Future work will need to
236 elucidate how the contractile properties of the apical membrane evolve as vessels
237 mature and are exposed to higher levels of blood pressure and shear stress. The
238 transition towards a multicellular organisation of endothelial tubes, and the observed

239 changes in cell shape and junction stability imply adaptations in the structure and
240 dynamics of the actin cytoskeleton. Understanding whether and how this plasticity of
241 the apical membrane and its underlying cortex is challenged in pathological
242 conditions, where vessels display altered perfusion and lack organised structure, has
243 the potential to provide deeper insight into mechanisms of vascular adaptation and
244 maladaptation.

- 246 1. Chen, Q. *et al.* Haemodynamics-driven developmental pruning of brain
247 vasculature in zebrafish. *PLoS Biol* **10**, e1001374 (2012).
- 248 2. Kochhan, E. *et al.* Blood flow changes coincide with cellular rearrangements
249 during blood vessel pruning in zebrafish embryos. *PLoS One* **8**, e75060
250 (2013).
- 251 3. Herwig, L. *et al.* Distinct cellular mechanisms of blood vessel fusion in the
252 zebrafish embryo. *Curr Biol* **21**, 1942-1948 (2011).
- 253 4. Lenard, A. *et al.* In vivo analysis reveals a highly stereotypic morphogenetic
254 pathway of vascular anastomosis. *Dev Cell* **25**, 492-506 (2013).
- 255 5. Potente, M., Gerhardt, H. & Carmeliet, P. Basic and therapeutic aspects of
256 angiogenesis. *Cell* **146**, 873-887 (2011).
- 257 6. Jakobsson, L. *et al.* Endothelial cells dynamically compete for the tip cell
258 position during angiogenic sprouting. *Nat Cell Biol* **12**, 943-953 (2010).
- 259 7. Pelton, J.C., Wright, C.E., Leitges, M. & Bautch, V.L. Multiple endothelial
260 cells constitute the tip of developing blood vessels and polarize to promote
261 lumen formation. *Development* **141**, 4121-4126 (2014).
- 262 8. Jin, S.W., Beis, D., Mitchell, T., Chen, J.N. & Stainier, D.Y. Cellular and
263 molecular analyses of vascular tube and lumen formation in zebrafish.
264 *Development* **132**, 5199-5209 (2005).
- 265 9. Strilic, B. *et al.* The molecular basis of vascular lumen formation in the
266 developing mouse aorta. *Dev Cell* **17**, 505-515 (2009).
- 267 10. Charpentier, M.S., Tandon, P., Trincot, C.E., Koutleva, E.K. & Conlon, F.L.
268 A distinct mechanism of vascular lumen formation in *Xenopus* requires
269 EGFL7. *PLoS One* **10**, e0116086 (2015).
- 270 11. Wang, Y. *et al.* Moesin1 and Ve-cadherin are required in endothelial cells
271 during in vivo tubulogenesis. *Development* **137**, 3119-3128 (2010).
- 272 12. Cunningham, C.C. Actin polymerization and intracellular solvent flow in cell
273 surface blebbing. *J Cell Biol* **129**, 1589-1599 (1995).
- 274 13. Keller, H. & Eggl, P. Protrusive activity, cytoplasmic compartmentalization,
275 and restriction rings in locomoting blebbing Walker carcinosarcoma cells are
276 related to detachment of cortical actin from the plasma membrane. *Cell Motil*
277 *Cytoskeleton* **41**, 181-193 (1998).
- 278 14. Paluch, E., Piel, M., Prost, J., Bornens, M. & Sykes, C. Cortical actomyosin
279 breakage triggers shape oscillations in cells and cell fragments. *Biophys J* **89**,
280 724-733 (2005).
- 281 15. Charras, G.T., Coughlin, M., Mitchison, T.J. & Mahadevan, L. Life and times
282 of a cellular bleb. *Biophys J* **94**, 1836-1853 (2008).
- 283 16. Charras, G. & Paluch, E. Blebs lead the way: how to migrate without
284 lamellipodia. *Nat Rev Mol Cell Biol* **9**, 730-736 (2008).
- 285 17. Martin-Belmonte, F. *et al.* PTEN-mediated apical segregation of
286 phosphoinositides controls epithelial morphogenesis through Cdc42. *Cell* **128**,
287 383-397 (2007).
- 288 18. Sauteur, L. *et al.* Cdh5/VE-cadherin promotes endothelial cell interface
289 elongation via cortical actin polymerization during angiogenic sprouting. *Cell*
290 *Rep* **9**, 504-513 (2014).
- 291 19. Phng, L.K. *et al.* Formin-mediated actin polymerization at endothelial
292 junctions is required for vessel lumen formation and stabilization. *Dev Cell* **32**,
293 123-132 (2015).

- 294 20. Kamei, M. *et al.* Endothelial tubes assemble from intracellular vacuoles in
295 *in vivo*. *Nature* **442**, 453-456 (2006).
- 296 21. Yu, J.A., Castranova, D., Pham, V.N. & Weinstein, B.M. Single-cell analysis
297 of endothelial morphogenesis *in vivo*. *Development* **142**, 2951-2961 (2015).
- 298 22. Iwasaki, T., Murata-Hori, M., Ishitobi, S. & Hosoya, H. Diphosphorylated
299 MRLC is required for organization of stress fibers in interphase cells and the
300 contractile ring in dividing cells. *Cell structure and function* **26**, 677-683
301 (2001).
- 302 23. Emelyanov, A. & Parinov, S. Mifepristone-inducible LexPR system to drive
303 and control gene expression in transgenic zebrafish. *Dev Biol* **320**, 113-121
304 (2008).
- 305 24. Tinevez, J.Y. *et al.* Role of cortical tension in bleb growth. *Proc Natl Acad Sci*
306 *USA* **106**, 18581-18586 (2009).
- 307 25. Davis, G.E. & Camarillo, C.W. An alpha 2 beta 1 integrin-dependent
308 pinocytic mechanism involving intracellular vacuole formation and
309 coalescence regulates capillary lumen and tube formation in three-dimensional
310 collagen matrix. *Exp Cell Res* **224**, 39-51 (1996).
- 311 26. Xu, K. *et al.* Blood vessel tubulogenesis requires Rasip1 regulation of GTPase
312 signaling. *Dev Cell* **20**, 526-539 (2011).
- 313 27. Martin, M. *et al.* PP2A regulatory subunit Balpha controls endothelial
314 contractility and vessel lumen integrity via regulation of HDAC7. *EMBO J* **32**,
315 2491-2503 (2013).
- 316

317 Acknowledgements

318

319 We thank members of the Vascular Biology and Vascular Patterning Laboratories for
320 helpful discussions. We thank the Cancer Research UK London Research Institute
321 Animal and Fish Facilities, and the Aquatic Facilities at the Max Delbrück Center for
322 Molecular Medicine and Vesalius Research Center for animal care. We thank Thomas
323 Surrey and Nicholas Cade for access to the inverted 3i Spinning Disk Confocal, and
324 Pieter Vanden Berghe for access to the Andor Spinning Disk Confocal of the Cell
325 Imaging Core facility at the Vesalius Research Center. We thank Gavin Kelly from
326 the Francis Crick Institute (London, UK) for help with statistics. V.G. is funded by
327 Cancer Research UK. L.-K.P. is funded by a HFSP Long-Term Fellowship. H.G. is
328 funded by Cancer Research UK, the Lister Institute for Preventive Medicine, a
329 European Research Council starting grant REshape [311719] and the Berlin Institute
330 of Health (BIH). Supported by the DZHK (German Center for Cardiovascular
331 Research) and by the BMBF (German Ministry of Education and Research).

332

333

334 Author contributions

335

336 V.G., L.-K.P. and H.G. designed the experiments. V.G. and L.-K.P. performed the
337 experiments and analysed the data. R.C. generated the *Tg(fli1ep:PLC δ -PH-RFP)*
338 zebrafish line. I.G. generated the *Tg(fli1ep:EGFP-CAAX)* zebrafish line. V.G. and
339 H.G. wrote the manuscript.

340

341

342 Competing financial interests

343

344 The authors declare no competing financial interests.

345

346 Figure legends

347

348 **Figure 1. Blood pressure drives unicellular and multicellular lumen expansion in**
349 **angiogenic sprouts**

350 a) Schematic illustration of unicellular and multicellular lumen formation in
351 angiogenic sprouts.

352 b) *Tg(kdr-l:ras-Cherry)^{s916}* embryos were imaged from 32 hpf. Black arrows, cell
353 junction. Magenta arrows, apical membrane. Time is in hours:minutes:seconds. Scale
354 bar is 10 μ m. Images are representative of 10 embryos analysed.

355 c) Mouse retinas were harvested at P6 and stained for ICAM-2, ZO-1 and Isolectin
356 IB₄. Isolectin IB₄ staining was used to draw the cell outline (white dotted line). White
357 arrow, unicellular membrane invagination. Scale bar is 10 μ m.

358 d) The number of endothelial sprouts with unicellular or multicellular lumens were
359 quantified in P6 mouse retinas stained for ICAM-2 and ZO-1 (n=487 sprouts from 9
360 retinas).

361 e) *Tg(kdr-l:ras-Cherry)^{s916}* embryos were imaged from 33 hpf after the addition of 4x
362 tricaine. Blood flow stopped after 20-25 minutes of treatment, leading to a decrease in
363 blood pressure noticeable through the decrease in diameter of the dorsal aorta
364 (double-headed arrow). At 48 hpf, embryos were returned to 1x tricaine and imaged
365 further. Magenta arrows, apical membrane. Magenta filling, lumen. Times are in
366 hours:minutes:seconds and correspond to the times after addition of 4x tricaine (left
367 panels) and after washout (right panels). Scale bar is 20 μ m. Images are representative
368 of 7 embryos analysed.

369

370 **Figure 2. Apical membrane undergoes inverse blebbing during lumen expansion**

371 a) Embryos with mosaic expression of EGFP-CAAX were imaged from 36 hpf.
372 Arrow in B, retracting bleb. Arrowheads in C, bleb necks. Arrow in D, lumen
373 collapse. Time is in hours:minutes:seconds. Scale bars are 10 μm (A,C,D) and 5 μm
374 (B). Images are representative of 7 embryos analysed.

375 b) A kymograph was generated along the magenta line in a, panel A. X axis, time (t)
376 in minutes. Y axis, distance (d) in μm . Black arrowheads, retracting blebs. White
377 arrowheads, non-retracting blebs.

378 c) Multicellular sprouts were imaged in *Tg(kdr-l:ras-Cherry)^{s916}* embryos with mosaic
379 expression of EGFP-CAAX from 32 hpf. Arrowheads, inverse blebs. Time is in
380 hours:minutes:seconds. Scale bar is 10 μm . Images are representative of 4 embryos
381 analysed.

382 d) Mouse retinas were collected at P6 and stained for ICAM-2, ZO-1 and Isolectin
383 IB₄. Isolectin IB₄ staining was used to draw the cell outline (white dotted line).
384 Arrow, constricted apical membrane. Arrowhead, lumen fragment. Scale bar is 10
385 μm .

386 e) The number of lumenised unicellular sprouts showing expanded, constricted or
387 disconnected apical membrane was quantified in P6 mouse retinas stained for ICAM-
388 2 and ZO-1 (n=57 sprouts from 9 retinas).

389

390 **Figure 3. Blood pressure drives inverse blebbing at the apical membrane of**
391 **angiogenic sprouts**

392 a) *Tg(fli1ep:EGFP-CAAX)* embryos were imaged from 33 hpf. Ablation was
393 performed at the base of the ISV to stop blood flow in the sprout (double-headed
394 arrow, ablated region). A kymograph was generated along the magenta line in A to
395 follow apical membrane dynamics before and after ablation. X axis, time (t) in

396 minutes. Y axis, distance (d) in μm . Arrowheads, inverse blebs. Scale bars are 10 μm .
397 Images are representative of 6 embryos analysed.

398 b) *Tg(kdr-l:ras-Cherry)^{s916}* embryos were imaged from 32 hpf in 1x tricaine, and then
399 treated with 4x tricaine. Blood flow stopped approximately 15 minutes after the start
400 of the treatment. After 30 minutes of treatment, embryos were washed with E3 buffer
401 and placed back in 1x tricaine. A kymograph was generated along the magenta line in
402 A to follow apical membrane dynamics. X axis, time (t) in minutes. Y axis, distance
403 (d) in μm . Arrowheads, inverse blebs. Arrows, remnants of apical membrane. Scale
404 bar is 10 μm . Images are representative of 5 embryos analysed.

405

406 **Figure 4. Endothelial cells retract inverse blebs by recruiting and contracting**
407 **actomyosin at the apical membrane**

408 a) *Tg(kdr-l:ras-Cherry)^{s916}* embryos with mosaic expression of Lifeact-EGFP were
409 imaged from 35 hpf. Dotted line, apical membrane. Arrow, expanding apical
410 membrane. Arrowhead, onset of F-actin polymerisation. C, cytoplasm. L, lumen.
411 Time is in hours:minutes:seconds. Scale bar is 5 μm . Images are representative of 5
412 embryos analysed.

413 b) Kymograph generated along the magenta line in a. X axis, time (t) in seconds. Y
414 axis, distance (d) in μm . Dotted line, apical membrane.

415 c) Embryos with mosaic expression of Myl9b-EGFP and Lifeact-mCherry were
416 imaged from 35 hpf. Arrow, onset of F-actin polymerisation. Arrowhead, onset of
417 Myosin-II recruitment. C, cytoplasm. E, extracellular space. L, lumen. Time is in
418 hours:minutes:seconds. Scale bar is 5 μm . Images are representative of 5 embryos
419 analysed.

420 d) Kymograph generated along the magenta line in c. X axis, time (t) in seconds. Y
421 axis, distance (d) in μm .

422 e) Embryos with mosaic expression of Myl9b-EGFP or Myl9bAA-EGFP and Lifeact-
423 mCherry were imaged from 34 hpf. Blebs growing on the lateral sides of expanding
424 lumens were assessed for their ability to retract within the maximum time necessary
425 for expansion and retraction (approximately 10 minutes, see Supplementary Fig.
426 1a,b). A multinomial log-linear model was used to test for association of bleb count in
427 the different categories with the mutation status (WT: n=102 blebs from 5 cells; AA:
428 n=161 blebs from 5 cells; data pooled from three independent experiments; $p=2.1\text{e-}$
429 13; ****, $p<0.0001$).

430 f) *Tg(kdr-l:ras-Cherry^{s916};fli1ep:Lifeact-EGFP)* embryos were imaged from 33 hpf.
431 Laser ablation was performed along a line spanning the entire thickness of the apical
432 membrane and its underlying cortex, at the tip of the growing lumen. Arrowhead, site
433 of ablation. Arrow, inverse bleb. C, cytoplasm. E, extracellular space. L, lumen. Scale
434 bar is 5 μm . Images are representative of 5 embryos analysed.

435 g-i) Lifeact-EGFP^{+wt} (g) and wild-type (h,i) mouse retinas were collected at P6 and
436 stained for ICAM-2 (g-i), non muscle (nm) Myosin II-A (h), and phospho Myosin
437 Light Chain 2 (pMLC2; i). Arrows show localisation of F-actin, nmMyosin II-A and
438 pMLC2 at the apical membrane. Images correspond to single confocal planes. Scale
439 bars are 10 μm .

440 j) Schematic illustration of inverse membrane blebbing. C, cytoplasm. L, lumen.

441

442 **Figure 5. Apical membrane contractility regulates lumen formation during**
443 **sprouting angiogenesis**

444 a) *Tg(kdr-l:ras-Cherry)^{s916}* embryos with mosaic expression of Myl9b-EGFP or
445 Myl9bAA-EGFP were analysed at 2 dpf. EGFP-positive ISVs were classified by eye
446 into three categories according to their level of EGFP expression (low, moderate,
447 strong) and screened for the presence of a lumen. A multinomial log-linear model was
448 used to test for association of cell count in the different categories with the mutation
449 status (WT: n=55 ISVs from 24 embryos; AA: n=31 ISVs from 9 embryos; data
450 pooled from three independent experiments; p=0.30 (low), p=0.11 (moderate),
451 p=0.0002 (high), p=0.00024 (total); **, p<0.01). EGFP-positive cells where the
452 presence or absence of a lumen could not be appreciated were referenced as
453 undetermined.

454 b) *Tg(kdr-l:ras-Cherry)^{s916}* embryos with mosaic expression of Myl9b-EGFP or
455 Myl9bAA-EGFP were imaged at 2 dpf. Arrowhead, disconnected lumen fragment.
456 Arrow, side lumen branch. Scale bars are 10 μ m. Images are representative of 6
457 embryos analysed.

458 c) *Tg(kdr-l:ras-Cherry)^{s916}* embryos with mosaic expression of Myl9bAA-EGFP were
459 imaged from 35 hpf. Arrowheads, lumen. Time is in hours:minutes:seconds. Scale bar
460 is 10 μ m. Images are representative of 3 embryos analysed.

461 d) Schematic model of lumen formation by inverse membrane blebbing during
462 sprouting angiogenesis *in vivo*. Haemodynamic forces generate a positive pressure
463 difference between the luminal and the cytoplasmic sides of the apical membrane (1).
464 Consequently, inverse blebs expand along the apical membrane at sites of weak
465 attachment of the cortex to the membrane (2). Following bleb expansion, F-actin
466 polymerises and myosin-II is recruited at the apical membrane of growing blebs (3).
467 Actomyosin contraction leads to bleb retraction (4), and selective bleb retraction
468 ensures unidirectional lumen expansion (5).

Methods

Mouse care and procedures

The following mouse (*Mus musculus*) strains were used in this study: C57BL/6 and Lifeact-EGFP²⁸. Animal procedures were performed in accordance with the United Kingdom's Home Office Animal Act 1986 under the authority of project license PPL 80/2391. Animals were analysed regardless of sex.

Retina dissection, immunofluorescence staining and imaging

Eyes were collected at post-natal day 6 (P6) and fixed in 4% paraformaldehyde (PFA) in phosphate buffer saline (PBS) for 1 hour at 4°C. Retinas were dissected, blocked in CBB buffer (0.5% Triton X-100, 1% bovine serum albumin (BSA), 2% sheep serum, 0.01% sodium deoxycholate, 0.02% sodium azide) for 2 hours at 4°C and incubated overnight at 4°C with the following primary antibodies diluted in 1:1 PBS:CBB at the indicated concentrations: ICAM-2 (1:400; BD Biosciences, Cat. #553326, lot #4213932), Phospho-Myosin Light Chain 2 (1:100; Cell Signalling, Cat. #3671), Non Muscle Myosin Heavy Chain II-A (1:100; Covance, Cat. #PRB-440P), ZO-1 (1:400; Life Technologies, Cat. #61-7300). Retinas were then washed three times for 10 minutes in PBS supplemented with 0.1% Tween-20 (PBST), and incubated for 2 hours at room temperature with secondary antibodies diluted in 1:1 PBS:CBB at the indicated concentrations: goat anti-rabbit Alexa Fluor® 488 (1:1000; Life Technologies, Cat. #A-11008) and goat anti-rat Alexa Fluor® 555 (1:1000; Life Technologies, Cat. #A-21434). Retinas were finally washed three times for 10 minutes with PBST, fixed for 10 minutes at room temperature in 4% PFA, and mounted in Vectashield (Vector Laboratories, H-1000). When needed, Isolectin

staining was performed by incubating the retinas overnight at 4°C with Isolectin GS-IB₄ Alexa Fluor® 647 (Life Technologies, Cat. #I32450) diluted 1:400 in PBlec buffer (1% Tween-20, 0.1 mM CaCl₂, 0.1 mM MgCl₂, 0.1 mM MnCl₂ in PBS, pH 6.8). Samples were imaged with an upright Carl Zeiss LSM 780 microscope using an Alpha Plan-Apochromat 63x/1.46 NA oil objective.

Fish maintenance and stocks

Zebrafish (*Danio rerio*) were raised and staged as previously described²⁹. The following transgenic lines were used: *Tg(kdr-l:ras-Cherry)*^{s916 30}, *Tg(fli1ep:EGFP)*^{y1 31}, *Tg(fli1ep:PLCδ-PH-RFP)*, *Tg(fli1ep:EGFP-CAAX)* and *Tg(fli1ep:Lifact-EGFP)*³².

Cloning, constructs and mosaic expression in zebrafish

All constructs were generated using the Tol2Kit³³ and the Multisite Gateway system (Life Technologies). The coding sequence of EGFP-CAAX was provided in the Tol2Kit; the sequence coding for the pleckstrin homology (PH) domain of PLCδ was a gift from Banafshé Larijani (University of the Basque Country, Spain); Lifact and Myl9b coding sequences were obtained from Riedl and colleagues²⁸ and Source Bioscience (clone I0038156), respectively. Dominant-negative Myl9b (Myl9bAA) was generated by substituting Thr18 and Ser19 by Ala using the QuikChange II Site-Directed Mutagenesis Kit (Agilent Technologies). The *fli1ep* promoter (gift from Nathan Lawson, University of Massachusetts Medical School, USA) was used to drive endothelial expression of PLCδ-PH-RFP, EGFP-CAAX, Lifact-EGFP and Lifact-mCherry fusion constructs. For inducible expression of Myl9b-EGFP and Myl9bAA-EGFP, the coding sequence for the LexPR transactivator was placed under

the *flilep* promoter, while Myl9b-EGFP and Myl9bAA-EGFP fusion constructs were placed under the LexA operator³⁴. Tol2 transposase mRNA was transcribed from the *pCS-TP* plasmid³⁵ using the SP6 mMACHINE Kit (Life Technologies). Embryos were injected at the one-cell stage with 100 pg of Tol2 transposase mRNA and 40 pg of plasmid DNA. Embryos injected with the *pTol2-flilep:LexPR* and *pTol2-lexOP:Myl9b-EGFP* or *pTol2-lexOP:Myl9bAA-EGFP* plasmids were dechorionated and treated from 26 hpf with 20 μ M Mifepristone (Sigma, M8046) in E3 buffer (5 mM NaCl, 0.17 mM KCl, 0.33 mM CaCl₂, 0.33 mM MgSO₄) to induce expression of the transgenes.

Live imaging

Embryos were dechorionated and anaesthetised with 0.16 mg/mL (1x) tricaine methanesulfonate (Sigma). Embryos were then mounted in 0.8% low melting point agarose (Life Technologies) and immersed in E3 buffer with 1x tricaine. When needed, heartbeat was inhibited by changing the medium for E3 buffer with 4x tricaine. Live imaging was performed on an inverted 3i Spinning Disk Confocal using a Zeiss C-Apochromat 63x/1.2 NA water immersion objective, on an upright 3i Spinning Disk Confocal using a Zeiss Plan-Apochromat 63x/1.0 NA water dipping objective, and on an inverted Andor Revolution 500 Spinning Disk Confocal using a Nikon Plan Apo 60x/1.24 NA water immersion objective.

Laser ablation

Laser ablations were performed on an upright 3i Spinning Disk Confocal fitted with a Zeiss Plan-Apochromat 63x/1.0 NA water dipping objective using an Ablate™ 532 nm pulse laser. Ablations were performed in single confocal planes along lines

spanning the entire thickness of the structures to be ablated (cell body, or membrane and underlying cortex). Laser was applied for 10 ms at 10-20% laser power. Ablation of the structures of interest was obtained by performing sequential laser cuts using increasing laser power (starting from 10% with 1% increments, up to 20%) at 5 to 10-second intervals.

Image analysis

Images were analysed using the Fiji software³⁶. Z-stacks were flattened by maximum intensity projection. XY drifts were corrected using the MultiStackReg plugin (B. Busse, NICHD). Fluorescence bleaching was corrected by Histogram Matching. Kymographs were generated using the MultipleKymograph plugin (J. Rietdorf and A. Seitz, EMBL). Contrast in all images was adjusted in Adobe Photoshop CS5.1 for visualisation purposes. All images are representative of the analysed data.

Statistical analysis

A multinomial log-linear model was used to test for association of bleb or cell count in different defined phenotypic categories with the cell mutation status (WT or AA). The null model was that count variation was only due to experimental batch. No statistical method was used to predetermine sample size. Zebrafish embryos were selected on the following pre-established criteria: normal morphology, beating heart, and presence of circulating red blood cells suggestive of blood flow. The experiments were not randomised. The investigators were not blinded to allocation during experiment and outcome assessment.

28. Riedl, J. *et al.* Lifeact mice for studying F-actin dynamics. *Nat Methods* **7**, 168-169 (2010).

29. Kimmel, C.B., Ballard, W.W., Kimmel, S.R., Ullmann, B. & Schilling, T.F. Stages of embryonic development of the zebrafish. *Dev Dyn* **203**, 253-310 (1995).
30. Hogan, B.M. *et al.* Ccbe1 is required for embryonic lymphangiogenesis and venous sprouting. *Nat Genet* **41**, 396-398 (2009).
31. Lawson, N.D. & Weinstein, B.M. In vivo imaging of embryonic vascular development using transgenic zebrafish. *Dev Biol* **248**, 307-318 (2002).
32. Phng, L.K., Stanchi, F. & Gerhardt, H. Filopodia are dispensable for endothelial tip cell guidance. *Development* **140**, 4031-4040 (2013).
33. Kwan, K.M. *et al.* The Tol2kit: a multisite gateway-based construction kit for Tol2 transposon transgenesis constructs. *Dev Dyn* **236**, 3088-3099 (2007).
34. Emelyanov, A. & Parinov, S. Mifepristone-inducible LexPR system to drive and control gene expression in transgenic zebrafish. *Dev Biol* **320**, 113-121 (2008).
35. Kawakami, K. *et al.* A transposon-mediated gene trap approach identifies developmentally regulated genes in zebrafish. *Dev Cell* **7**, 133-144 (2004).
36. Schindelin, J. *et al.* Fiji: an open-source platform for biological-image analysis. *Nat Methods* **9**, 676-682 (2012).

Supplementary Figure legends

Supplementary Figure 1 (related to Figure 2)

a-e) *Tg(kdr-l:ras-Cherry)^{s916}* embryos with mosaic expression of Lifeact-EGFP were used to measure expansion time (a), retraction time (b), expansion speed (c) and retraction speed (d) in relation to bleb size (n=31 blebs from 3 cells). Dots in (a-d) correspond to single blebs. (e) shows mean and standard deviation for each property. Values for classical blebs come from ¹.

f) *Tg(fli1ep:EGFP;fli1ep:PLC δ -PH-RFP)* embryos were imaged from 35 hpf. Arrowhead, inverse bleb. C, cytoplasm. E, extracellular space. L, lumen. Time is in hours:minutes:seconds. Scale bar is 5 μ m.

Supplementary Figure 2 (related to Figure 4)

a) Embryos with mosaic expression of Myl9b-EGFP and Lifeact-mCherry were imaged at 2 dpf. Arrowheads show co-localisation of F-actin and Myosin-II at cell junctions (A), at the apical membrane (B), and at the base of filopodia (C). Scale bars are 10 μ m. Images are representative of 6 embryos analysed.

b) *Tg(kdr-l:ras-Cherry)^{s916}* embryos with mosaic expression of Myl9b-EGFP were imaged from 34 hpf. Dotted line, apical membrane. Arrow, expanding apical membrane. Arrowhead, onset of Myosin-II recruitment. C, cytoplasm. E, extracellular space. L, lumen. Time is in hours:minutes:seconds. Scale bar is 5 μ m. Images are representative of 3 embryos analysed.

c) Kymograph generated along the magenta line in b. X axis, time (t) in seconds. Y axis, distance (d) in μ m.

Supplementary Video legends

Supplementary Video 1 (related to Figure 2a). Apical membrane undergoes inverse blebbing during lumen expansion in sprouting ISVs

Time-lapse series of an endothelial sprout with mosaic expression of EGFP-CAAX imaged from 36 hpf. The apical membrane shows inverse blebs as the lumen expands into the sprout (black arrow). The red arrow shows a disconnected lumen fragment originating from the collapse of the lumen. Time is in hours:minutes:seconds.

Supplementary Video 2 (related to Supplementary Figure 1f). Early apical determinants localise at the apical membrane during inverse blebbing

Time-lapse series of an endothelial sprout expressing cytoplasmic EGFP (left panel, green) and a PLC δ -PH-RFP reporter for PIP₂ (right panel, magenta) imaged from 35 hpf. The apical membrane retains apical markers (PIP₂) as it expands (white arrow). Time is in hours:minutes:seconds.

Supplementary Video 3 (related to Figure 2c). Inverse membrane blebbing drives multicellular lumen expansion in sprouting ISVs

Time-lapse series of an endothelial sprout with mosaic expression of EGFP-CAAX (left panel, green) and expression of mCherry-CAAX (right panel, magenta) imaged from 32 hpf. Inverse blebbing occurs simultaneously in both cells forming the ISV as the lumen expands (white arrows). Time is in hours:minutes:seconds.

Supplementary Video 4 (related to Figure 3a). Interruption of blood flow by laser ablation inhibits inverse blebbing at the apical membrane of sprouting ISVs

Time-lapse series of an endothelial sprout expressing EGFP-CAAX imaged from 33 hpf. Laser ablation was performed along a line spanning the entire thickness of the vessel at the place indicated by the red arrow, and at the time indicated. Ablation led to an immediate loss of the inverse blebs at the apical membrane and to gradual regression of the lumen (black arrow). Time is in hours:minutes:seconds.

Supplementary Video 5 (related to Figure 3b). Interruption of blood flow by tricaine treatment inhibits inverse blebbing at the apical membrane of sprouting ISVs

Time-lapse series of an endothelial sprout expressing mCherry-CAAX imaged from 34 hpf, before, during and after treatment with 4x tricaine. Blood flow stops about 15-20 minutes after addition of 4x tricaine, leading to a loss of the inverse blebs at the apical membrane. Black arrows show expansion of the apical membrane by inverse blebbing before treatment with 4x tricaine and after washout. Time is in hours:minutes:seconds.

Supplementary Video 6 (related to Figure 4a,b). F-actin polymerises around inverse blebs as they retract

Time-lapse series of an endothelial sprout with mosaic expression of Lifeact-EGFP (left panel, green) and mCherry-CAAX (right panel, magenta) imaged from 35 hpf. F-actin polymerises around inverse blebs as they retract. Time is in hours:minutes:seconds.

Supplementary Video 7 (related to Figure 4f). Laser ablation of the cell cortex at the apical membrane of growing lumens leads to the expansion of inverse blebs

Time-lapse series of an endothelial sprout expressing Lifeact-EGFP (left panel, green) and mCherry-CAAX (right panel, magenta) imaged from 33 hpf. Laser ablation of the cell cortex was performed along the indicated black/white line and led to the expansion of a bleb that later retracted (white arrow). Time is in hours:minutes:seconds.

Supplementary Video 8 (related to Supplementary Figure 5c). Apical contractility is required for lumen expansion in sprouting ISVs

Time-lapse series of an endothelial sprout with mosaic expression of Myl9bAA-EGFP (left panel, green) and mCherry-CAAX (right panel, magenta) imaged from 35 hpf. The cell expressing Myl9bAA fails to lumenise from the ventral part of the ISV. Lumen pushes into the cell from the dorsal longitudinal anastomotic vessel (DLAV) but fails to expand (white arrows). Time is in hours:minutes:seconds.

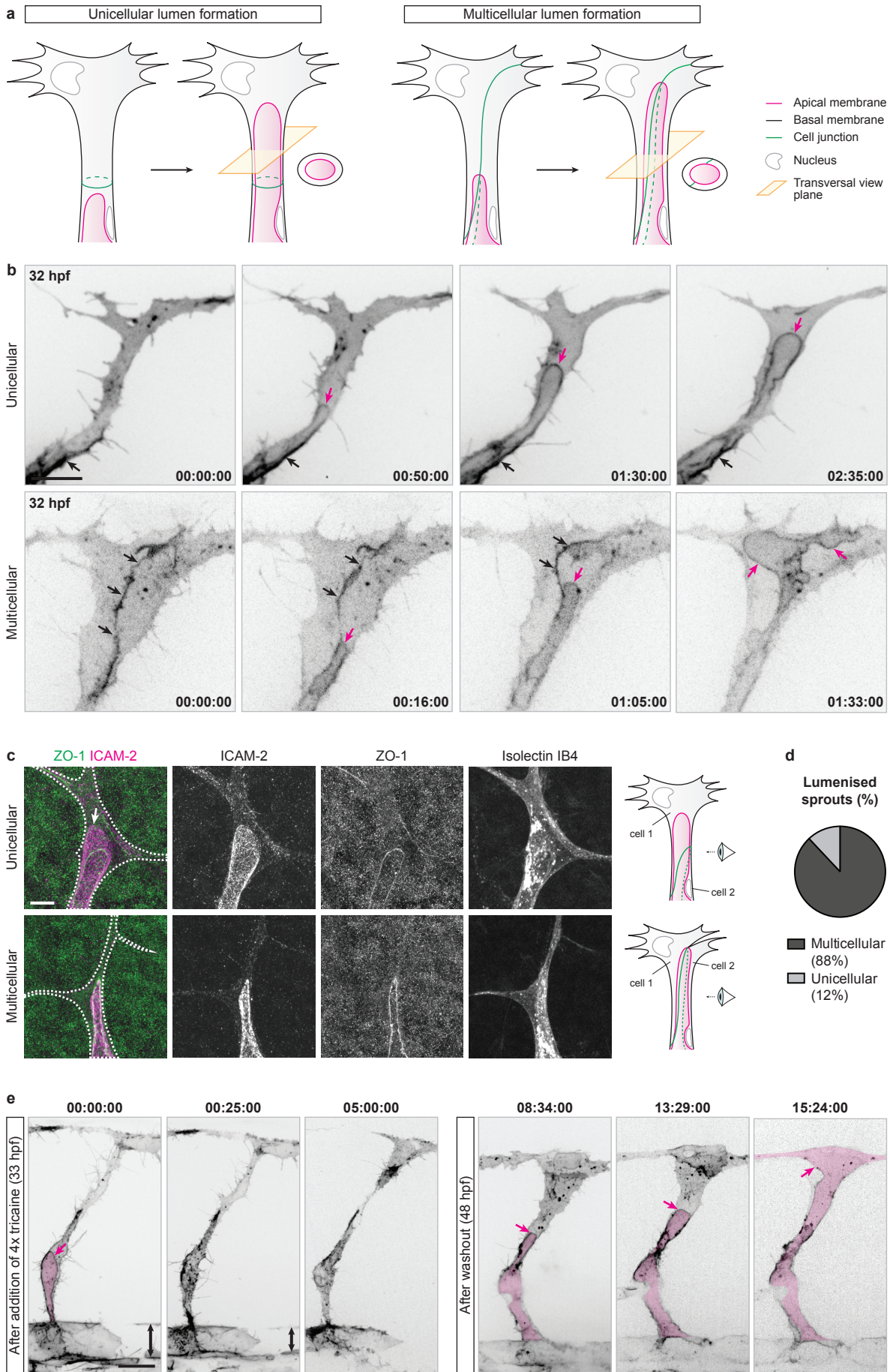
Supplementary Video 9 (related to Figure 5b). Endothelial cells with decreased apical contractility show uncontrolled blebbing

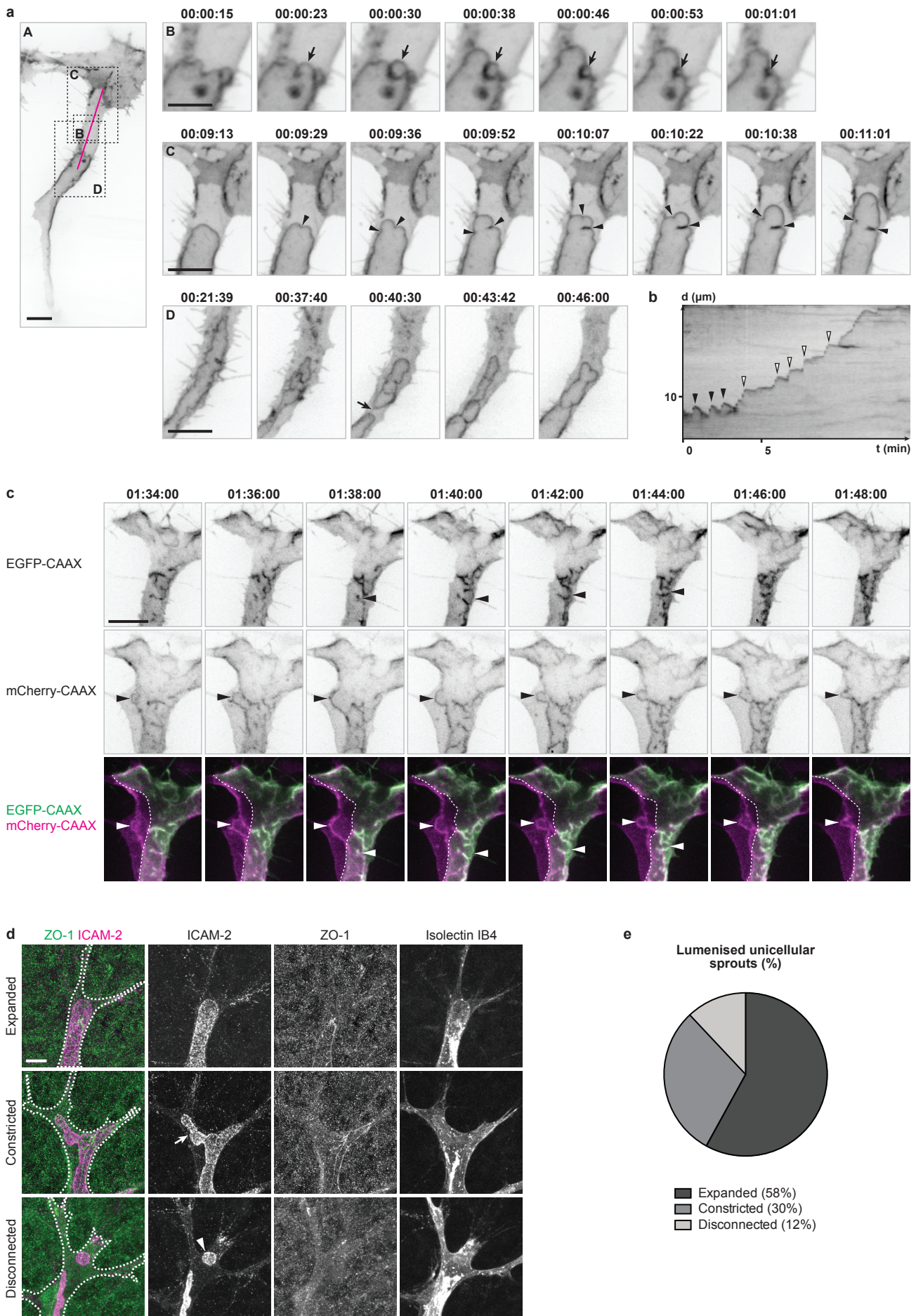
Time-lapse series of an endothelial sprout with mosaic expression of Myl9bAA-EGFP (left panel, green) and mCherry-CAAX (right panel, magenta) imaged from 48 hpf. The apical membrane undergoes excessive and uncoordinated blebbing and fails to expand. Time is in hours:minutes:seconds.

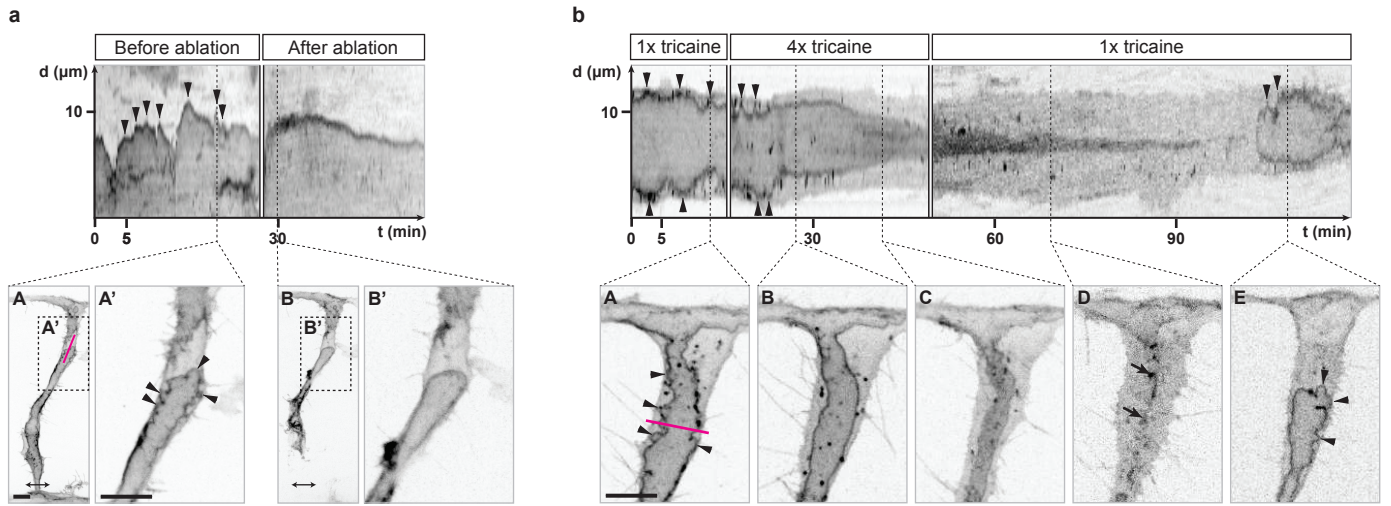
Supplementary Video 10 (related to Figure 5b). Partially lumenised endothelial cells with decreased apical contractility show side lumen branches

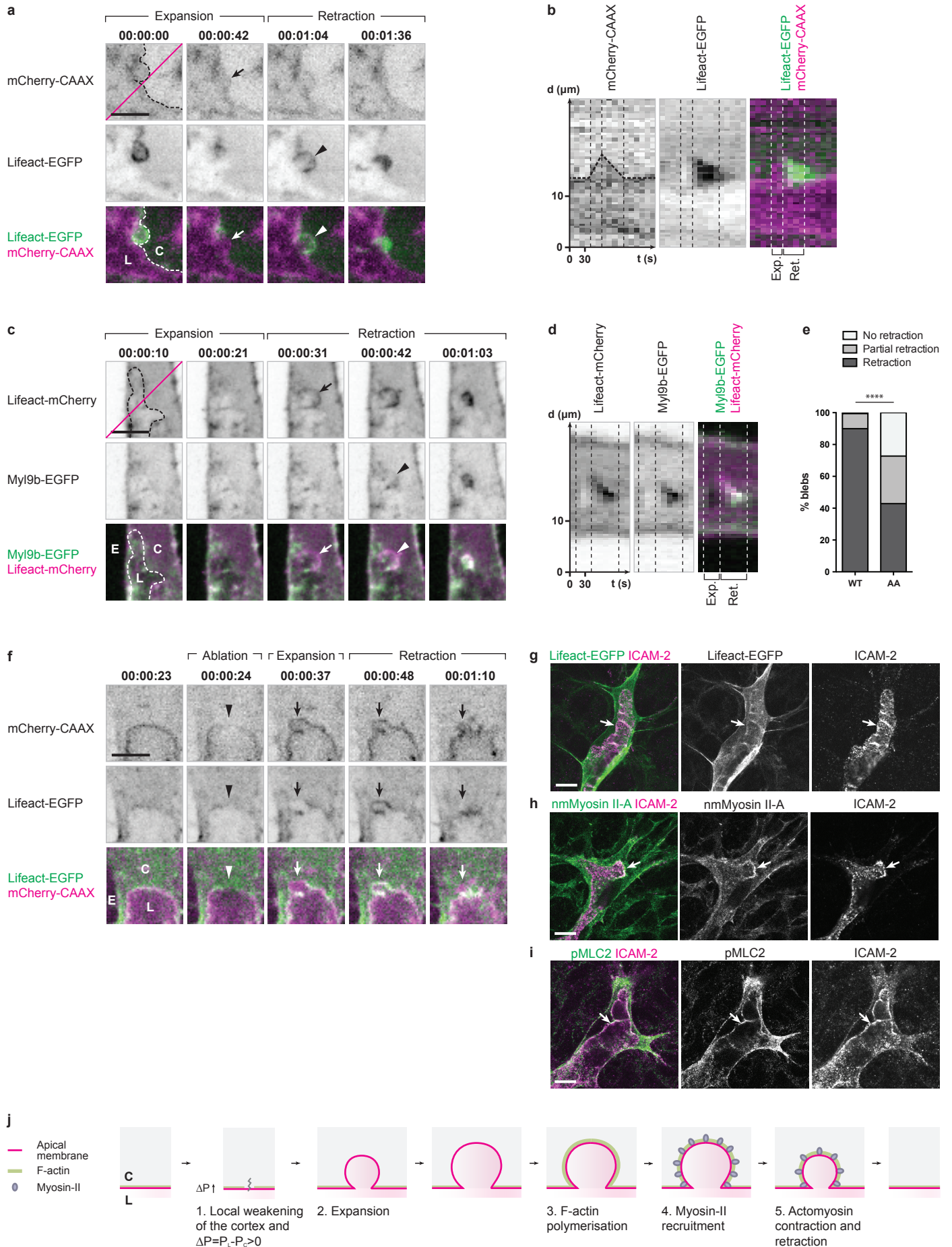
Time-lapse series of an endothelial sprout with mosaic expression of Myl9bAA-EGFP (left panel, green) and mCherry-CAAX (right panel, magenta) imaged from 52 hpf. The ISV is dilated and shows side lumen branches that fail to retract (white arrows). Time is in hours:minutes:seconds.

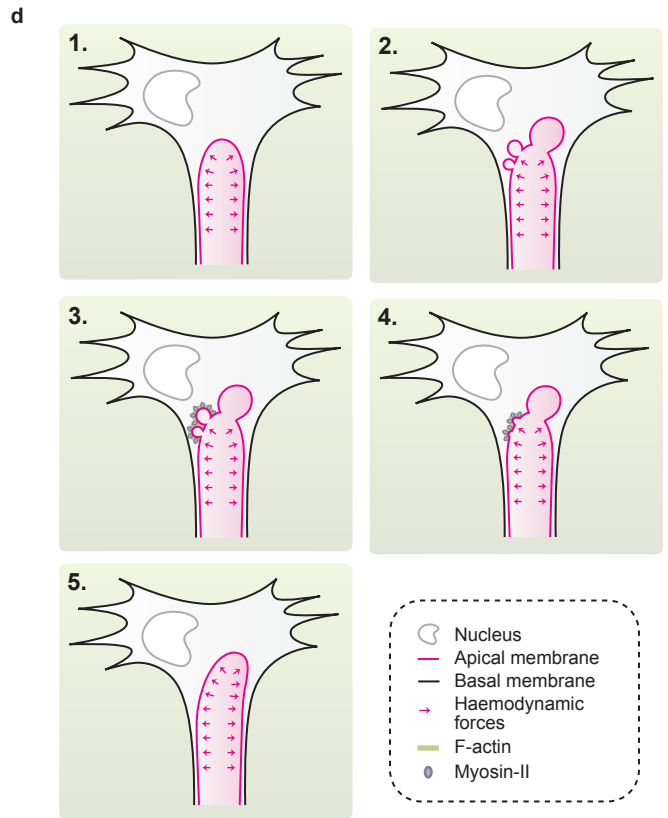
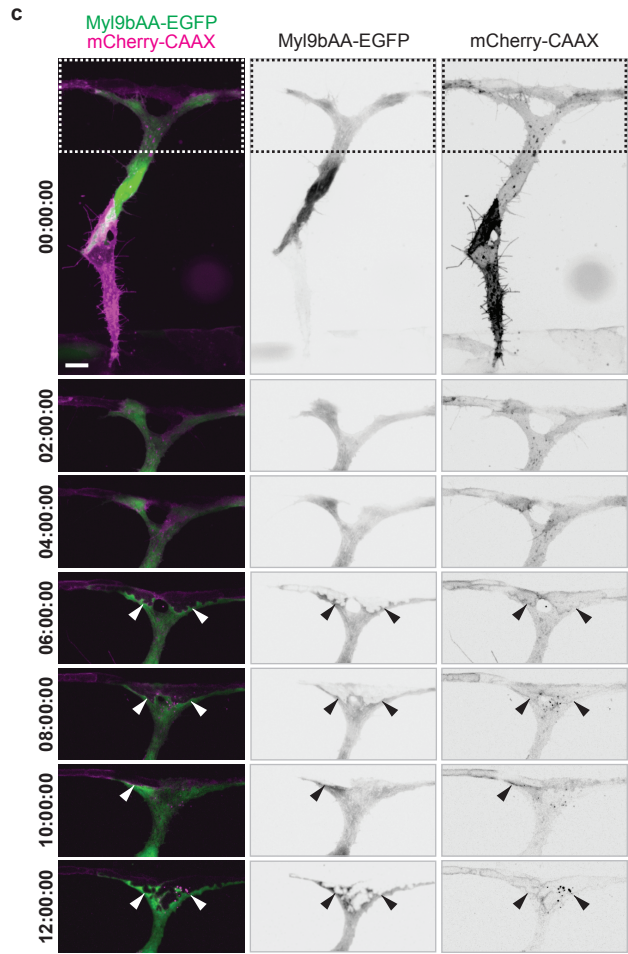
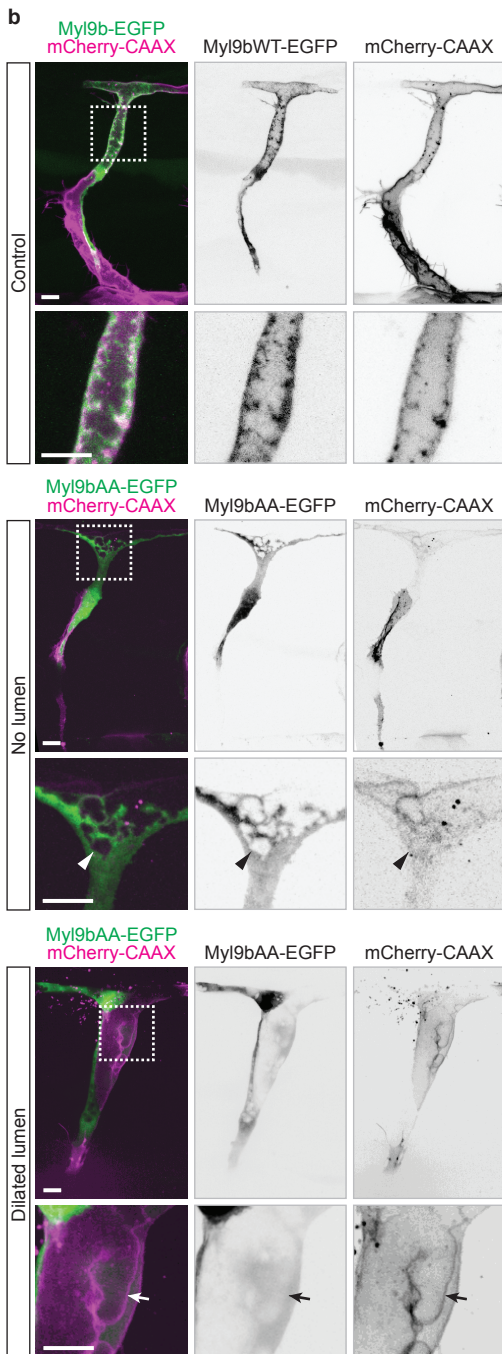
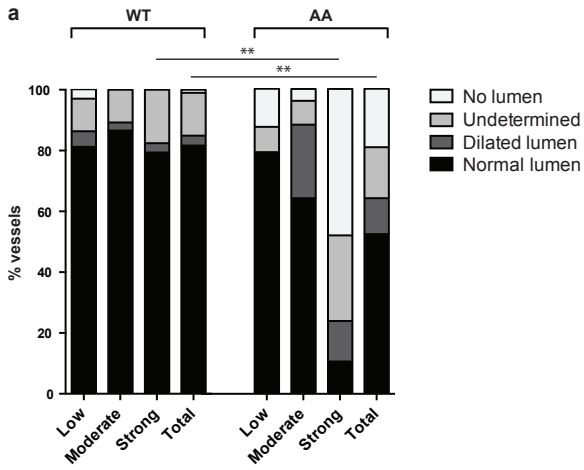
1. Charras, G.T., Coughlin, M., Mitchison, T.J. & Mahadevan, L. Life and times of a cellular bleb. *Biophys J* **94**, 1836-1853 (2008).

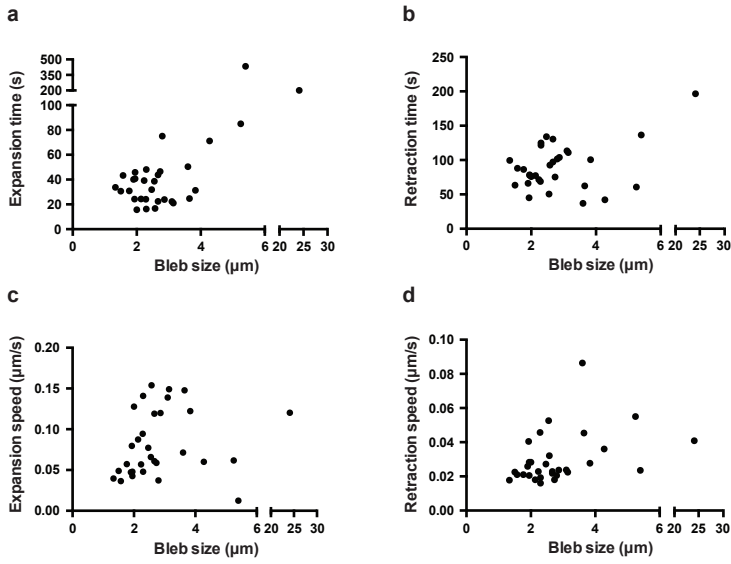












e

	Inverse blebs	Classical blebs
Bleb size (μm)	3.4 ± 4	2
Expansion time (s)	55 ± 78	30
Expansion speed ($\mu\text{m/s}$)	0.08 ± 0.04	0.25
Retraction time (s)	90 ± 34	120
Retraction speed ($\mu\text{m/s}$)	0.03 ± 0.01	0.03

